

Probing intermediate-mass black hole binaries with the Lunar Gravitational-wave Antenna

Hanlin Song^{1*}, Han Yan^{2,3}, Yacheng Kang^{2,3}, Xian Chen^{2,3}, Junjie Zhao⁴, Lijing Shao^{3,5*}

¹School of Physics, Peking University, Beijing, 100871, China.

²Department of Astronomy, School of Physics, Peking University, Beijing, 100871, China.

³Kavli Institute for Astronomy and Astrophysics, Peking University, Beijing, 100871, China.

⁴Institute for Gravitational Wave Astronomy, Henan Academy of Sciences, Zhengzhou, 450046, Henan, China.

⁵National Astronomical Observatories, Chinese Academy of Sciences, Beijing, 100012, China.

*Corresponding author(s). E-mail(s): lshao@pku.edu.cn;

Abstract

New concepts for observing the gravitational waves (GWs) using a detector on the Moon, such as the Lunar Gravitational-wave Antenna (LGWA), have gained increasing attention. By utilizing the Moon as a giant antenna, the LGWA is expected to detect GWs in the frequency range from 1 millihertz (mHz) to several hertz, with optimal sensitivity in the decihertz band. Despite the debated formation and evolution channel of intermediate-mass black holes (IMBHs) with masses in the range of $[10^2, 10^5] M_\odot$, binary systems containing at least one IMBH are widely believed to generate GWs spanning from mHz to a few Hz, making them a key scientific target for the LGWA. We explore the detectability of IMBH binaries with the LGWA in this work. The LGWA is more sensitive to nearby binaries (i.e. with redshift $z \lesssim 0.5$) with the primary mass $m_1 \in [10^4, 10^5] M_\odot$, while it prefers distant binaries (i.e. $z \gtrsim 5$) with $m_1 \in [10^3, 10^4] M_\odot$. Considering a signal-to-noise ratio threshold of 10, our results imply that the LGWA can detect IMBH binaries up to $z \sim O(10)$. We further show that the LGWA can constrain the primary mass with relative errors $\lesssim 0.1\%$ for binaries at $z \lesssim 0.5$. Furthermore, we show that the IMBH binaries at $z \lesssim 0.1$ can be used to constrain redshift with relative errors $\lesssim 10\%$, and those with $m_1 \in [10^4, 10^5] M_\odot$ can be localized by the LGWA to be within $O(10) \text{ deg}^2$.

1 Introduction

On September 14, 2015, the first gravitational-wave (GW) event was detected by the ground-based Laser Interferometer Gravitational-wave Observatory (LIGO) [1]. More recently, several pulsar timing arrays (PTAs) have reported intriguing evidence of the Hellings-Downs correlation from GW signals in the nanohertz band, including the North American Nanohertz Observatory for Gravitational waves (NANOGrav) [2, 3], the European PTA (EPTA) along with the Indian PTA (InPTA) [4–6], the Parkes PTA (PPTA) [7, 8], and the Chinese PTA (CPTA) [9]. Additionally, numerous other GW observatories are currently under investigation. These include next-generation (XG) ground-based detectors such as the Einstein Telescope (ET) [10] and the Cosmic Explorer (CE) [11], as well as space-borne detectors such as LISA [12], Taiji [13], TianQin [14], and DECIGO [15].

Recently, the new Moon-based detectors, such as the Lunar Gravitational-wave Antenna (LGWA) [16, 17], have gained increasing attention. When GWs pass by the Moon, it will vibrate, behaving like a giant antenna. The LGWA aims to deploy an array of inertial sensors in the Moon’s permanently shadowed regions to monitor its response. Given the exceptionally quiet and thermally stable environment of the permanently shadowed regions on the Moon, the LGWA is expected to observe GWs in the frequency range from 1 millihertz (mHz) to several hertz (Hz), with the optimal sensitivity in the decihertz band. It will bridge the gap between space-borne detectors with their optimal sensitivity at the mHz band like LISA, Taiji, and TianQin, and ground-based detectors like CE and ET with their optimal sensitivity at the audio band. Meanwhile, parallel design of a Moon-based detector was proposed by Li et al. [18] to make use of Chinese lunar exploration project, and it becomes a good supplement to other projects.

On the other hand, the intermediate-mass black holes (IMBHs) with masses between $10^2 M_\odot$ and $10^5 M_\odot$ are theoretically believed to play a crucial role in understanding the evolution of black holes and dynamics of stellar systems [19].

The existence of IMBHs is indicated by electromagnetic observations in globular clusters, ultraluminous X-ray sources, and dwarf galaxies [20]. With equipment of ground-based, space-borne, and Moon-based GW detectors, the binary systems of IMBHs can be observed through GW experiments. Due to the wide mass range of IMBHs, the inspiral, merger, and ringdown phases of their binary coalescence can be observed across the mHz to audio bands [21]. Recent studies have explored the detectability of IMBHs across different frequency bands: in the mHz range with LISA [22–25], in the decihertz range with DECIGO [26], and in the audio band with current [25, 27–29] and XG [23, 30, 31] ground-based GW detectors. Given that the Moon-based GW detectors have the optimal sensitivity in the decihertz band, the IMBHs also become a potentially key science target of those projects [16–18].

In this work, we focus on the detectability of IMBH binaries with quasi-circular orbits and aligned spins with the LGWA. Following the approach by Reali et al. [31], we perform a parameter scan with straightforward priors to generate the masses and redshifts of IMBH binaries. We then calculate the distribution of signal-to-noise ratios (SNRs) with different masses and redshifts for IMBH binaries. Using the Fisher information matrix (FIM) method, we calculate the relative parameter inference errors for some key parameters, such as the primary mass and redshift. We also calculate the localization capability of LGWA on IMBH binaries.

This paper is arranged as follows. In Sec. 2, we introduce the methodology and settings adopted in this work, including the parameter priors of IMBH binaries, the GW waveform template, the LGWA configuration, and a brief introduction of the FIM method. In Sec. 3, we present our results on the detectability of IMBH binaries by the LGWA. Finally, we conclude in Sec. 4. Throughout the paper, we adopt natural units $G = c = 1$.

2 Settings and Methods

In this section, we outline the settings and methods adopted in this work. In Sec. 2.1, we describe the parameter priors of IMBH binaries. In Sec. 2.2, we introduce the waveform model and the LGWA configurations. In Sec. 2.3, we briefly discuss the FIM method for parameter estimation.

2.1 Priors for the population of IMBH binaries

For the IMBH binary systems with aligned spins and quasi-circular orbits, the GW signals from them are described with 11 free parameters,

$$\theta = \{m_1, m_2, \chi_{1z}, \chi_{2z}, D_L, \alpha, \delta, \psi, \iota, \phi_c, t_c\}, \quad (1)$$

where m_1 and m_2 are source-frame binary masses of the two components, χ_{1z} and χ_{2z} are their dimensionless spin components which parallel with the orbital angular momentum, D_L is the luminosity distance of the source, α and δ are the right ascension and declination angles respectively, ι and ψ are the inclination angle the polarization angle respectively, and ϕ_c and t_c are the coalescence phase and time respectively.

Given the debated astrophysical star formation rate and merger rate for IMBHs, we follow Reali et al. [31] to adopt sample parameter priors of IMBHs which span the parameter space. As shown in Table 1, the source-frame primary mass is sampled logarithmically uniform from $m_1 \in [10^2, 10^5] M_\odot$, while the secondary mass is sampled logarithmically uniform from $m_2 \in [10 M_\odot, m_1]$. Meanwhile, the mass ratio $q = m_1/m_2 \in [1, 10]$ is further imposed in this work to guarantee the accuracy of the waveform model [31, 32]. We consider IMBH binaries which are fixed at six representative redshifts, $z \in \{0.05, 0.1, 0.5, 1, 5, 10\}$, to cover both nearby and distant cases. The luminosity distance D_L is then obtained using the Λ CDM cosmology model. The four angles α , $\cos \delta$, ψ , and $\cos \iota$, follow the uniform distributions $\mathcal{U}[0, 2\pi)$, $\mathcal{U}[-1, 1]$, $\mathcal{U}[0, \pi]$, and $\mathcal{U}[-1, 1]$, respectively. The priors for the coalescence phase, coalescence time, and two aligned spins are fixed to zero for all cases.

Table 1 Parameter priors of IMBH binaries.

Parameter	Priors
m_1	$[10^2, 10^5] M_\odot$ in log-uniform
m_2	$[10 M_\odot, m_1]$ in log-uniform
z	$\{0.05, 0.1, 0.5, 1, 5, 10\}$
α	$\mathcal{U}[0, 2\pi)$
$\cos \delta$	$\mathcal{U}[-1, 1]$
ψ	$\mathcal{U}[0, \pi]$
$\cos \iota$	$\mathcal{U}[-1, 1]$
ϕ_c	0
t_c	0
$\chi_{1z,2z}$	0

2.2 Waveform model and detectors

The detected GW strain is described as [33],

$$h = h_+ \vec{e}_+ : \vec{d} + h_\times \vec{e}_\times : \vec{d}, \quad (2)$$

where h_+ and h_\times are the ‘+’ and ‘ \times ’ polarization components of the GW respectively, \vec{e}_+ and \vec{e}_\times are the corresponding polarization tensors respectively, and \vec{d} is the response tensor of the detector.

Unlike current ground-based ‘‘L’’ shape laser interferometer type detectors like LIGO, Virgo, and KAGRA, the detection principle of LGWA has significant differences [16, 17, 34]. When a GW passes the Moon, its surface displacements can be measured by several seismometers of the LGWA. With the long-wavelength approximation, the response tensor of a seismometer is written as [35],

$$\vec{d} = \vec{e}_n \otimes \vec{e}_1, \quad (3)$$

where \vec{e}_n is the direction of the surface normal vector at the seismometer, and \vec{e}_1 is the direction of displacement measured by the seismometer. For a more realistic situation, the complete result of the response tensor is somewhat more complicated, including different contributions of radial and horizontal vibrations [36]. Thus, Eq. (3) can be regarded as a simplified case in which the radial response function is just two times of the horizontal response function, as shown in Eq. (7) in Yan et al. [36].

We use the IMRPhenomXHM waveform template [32] to generate h_+ and h_\times . Additionally, we employ the GWFish package [35] to calculate the GW strain projected onto the seismometer. Note that GWFish also takes into considerations the orbital motion of the Moon around the Earth, as well as the motion of the Earth-Moon system around the Sun during the detection period. We focus on the GW frequency band ranging from 10^{-3} Hz to 4 Hz. Additionally, 20,000 points are evenly spaced on a logarithmic scale for each signal. Furthermore, we utilize the default LGWA detector in GWFish, which consists of an array of four stations deployed in the Moon’s permanently shadowed regions. Each station is equipped with two horizontal Lunar inertial GW sensors, which measure the two orthogonal surface displacements [16, 17, 34]. The mission duration of the LGWA is expected to be 10 years. Thus, GW signals with time durations longer than 10 years are truncated at a low-frequency end via [35],

$$t(f) = t_c - \frac{5}{256 \mathcal{M}_c^{5/3}} (\pi f)^{-8/3}, \quad (4)$$

where \mathcal{M}_c is the chirp mass.

2.3 Fisher information matrix

Under the linear-signal approximation and assuming Gaussian and stationary noise, the posterior distribution of GW parameters becomes [37, 38],

$$p(\boldsymbol{\theta}) \sim e^{-\frac{1}{2} \Gamma_{ij} \Delta \theta_i \Delta \theta_j}, \quad (5)$$

where Γ_{ij} is the FIM and can be calculated as,

$$\Gamma_{ij} \equiv \left\langle \partial_{\theta_i} h(\boldsymbol{\theta}; f), \partial_{\theta_j} h(\boldsymbol{\theta}; f) \right\rangle. \quad (6)$$

Note that the inner product for two quantities $A(\boldsymbol{\theta}; f)$ and $B(\boldsymbol{\theta}; f)$ is defined as,

$$\langle A, B \rangle = 2 \int_0^\infty df \frac{A(\boldsymbol{\theta}; f) B^*(\boldsymbol{\theta}; f) + A^*(\boldsymbol{\theta}; f) B(\boldsymbol{\theta}; f)}{S_n(f)}, \quad (7)$$

where $S_n(f)$ is the one-sided power spectrum density (PSD) of the detector. The matched-filtering SNR for a GW event is calculated as,

$$\text{SNR} = \sqrt{\langle h, h \rangle}. \quad (8)$$

We also use the GWFish package for FIM calculations.

3 Results

With the definition of SNR shown in Eq. (8), the characteristic strains for a GW event h_c and the characteristic noise h_n can be defined as [39],

$$\begin{aligned} h_c &= 2f|h|, \\ h_n &= \sqrt{f S_n}. \end{aligned} \quad (9)$$

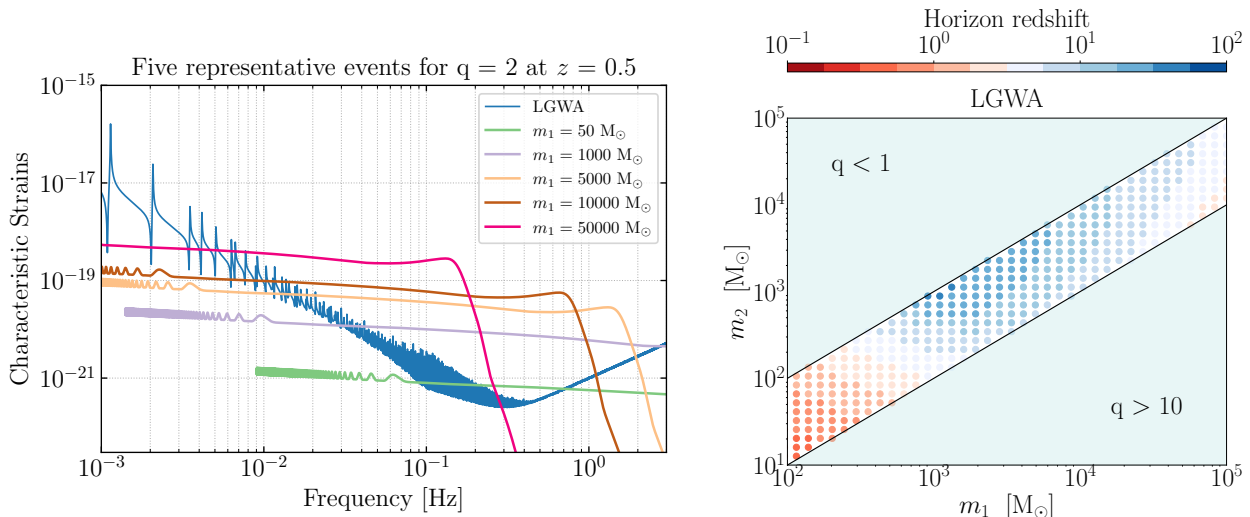


Fig. 1 The left panel shows the characteristic strain h_c for five representative events with different primary masses. The characteristic noise h_n of the LGWA is presented in blue line. All events are fixed at $z = 0.5$ with a mass ratio $q = 2$. The right panel shows the horizon redshift with a detection threshold $\text{SNR} = 10$. The region with mass ratio $q < 1$ is shaded for the requirement of $m_1 \geq m_2$, while the one with $q > 10$ is shaded for the applicability of the waveform model. For both panels, the four free angles in Table 1 are fixed to $\alpha = \pi/4$, $\cos \delta = 1/2$, $\psi = \pi/4$, and $\cos \iota = 1$.

In the left panel of Fig. 1, we plot the characteristic strains for five representative events of IMBH binaries and the characteristic sensitivity of LGWA. These events are put at $z = 0.5$ with five different primary masses $m_1 \in \{50, 1000, 5000, 10000, 50000\} M_\odot$. Additionally, the mass ratio is fixed to $q = 2$, and the four free angle parameters are fixed to $\alpha = \pi/4$, $\cos \delta = 1/2$, $\psi = \pi/4$, and $\cos \iota = 1$. As we can see, there exists a low-frequency cut off for lighter binaries, which is determined by the assumed maximum observation time of 10 years. The sinusoidal fluctuation at the low-frequency band actually arises from the orbital motion of the Moon around our Earth, as well as the motion of the Earth-Moon system around the Sun. With the primary mass increasing, the amplitude of GW signal increases, while the chirp frequency decreases. In the right panel of Fig. 1, we plot the horizon redshift for IMBH binaries with mass ratio between 1 and 10. The four angles are also fixed as in the left panel. The detection threshold is chosen as $\text{SNR} = 10$. We can clearly see that the binaries with primary mass $m_1 \in [10^3, 10^4] M_\odot$ have the best performance, which can be detected with a horizon redshift of $z \sim \mathcal{O}(10)$. These results are consistent with Ajith et al. [17].

Then we calculate the angle-averaged SNR for IMBHs at $z \in \{0.05, 0.1, 0.5, 1, 5, 10\}$. The results are shown in Fig. 2. For each point in the figure, we generate 1000 events with the corresponding m_1 , m_2 , and z values, while the four free angle parameters α , $\cos \delta$, ψ , and $\cos \iota$ are randomly drawn from the uniform priors in Table 1. The angle-averaged SNR is obtained by taking the average of the results from 1000 events. We find that all events can be detected at $z \lesssim 0.5$. However, at redshift $z \gtrsim 1$, the binaries with primary mass $m_1 \in [10^2, 10^3] M_\odot$ and $m_1 \in [10^4, 10^5] M_\odot$ show less detection efficiency. The angle-averaged SNRs fall below 10 for binaries at $z = 10$. It is interesting to note that for nearby binaries (i.e. $z \lesssim 0.5$), the binaries with $m_1 \in [10^4, 10^5] M_\odot$ show better performance. For example, at $z = 0.05$ or $z = 0.1$, binaries with $m_1 \in [10^4, 10^5] M_\odot$ can be detected with angle-averaged $\text{SNR} > \mathcal{O}(10^3)$, while for distant systems (i.e. $z \gtrsim 5$), binaries with $m_1 \sim [10^3, 10^4] M_\odot$ show better performance. This phenomenon arises due to the sensitivity profile of LGWA in the decihertz band. In Fig. 3, we plot the evolution of SNR with luminosity distance for each of the above five representative events in Fig. 1. The pink line denotes the binary system with $m_1 = 50000 M_\odot$, while the light orange line denotes the system with $m_1 = 5000 M_\odot$. As the luminosity distance increases, the LGWA becomes sensitive first to heavier systems and then to lighter systems. The turning point happens around $D_L \sim 10^4$ Mpc, which corresponds to $z \sim 1.5$ in the Λ CDM cosmology model. The SNR evolution for systems with other primary mass are also consistent with the results shown in Fig. 2. It is worth noting that the variation in detection sensitivity with source-frame mass and redshift can be mitigated by converting m_1 in Fig. 2 to detector-frame mass. For instance, in the cases of $z = 5$ and $z = 10$, the detector-frame mass will be magnified by approximately $\sim \mathcal{O}(10)$, whereas other cases remain almost unaffected.

In the following, we estimate the relative errors for m_1 , z , and the 90% sky localization uncertainty of IMBH binaries with the LGWA. In Fig. 4, we show the angle-averaged relative errors of the primary mass $\Delta m_1/m_1$ at different redshifts. For nearby binaries (i.e. $z \lesssim 0.5$), the primary mass can be measured with accuracy better than 0.1%. For binaries at $z = 1$, the primary mass can be measured with uncertainty less than 1% for most cases. However, for distant binaries (i.e. $z \gtrsim 5$), the primary mass can only be measured with lower accuracy, typically worse than 10% across most detectable regions. Figure 5 shows results for angle-averaged relative error of the redshift, $\Delta z/(1+z)$. For binaries at $z \lesssim 0.1$, the redshift can be constrained with relative errors $\lesssim 10\%$. For binaries at $z = 0.05$, the redshift can be constrained better than 1%. However, for binaries at $z \gtrsim 0.5$, the redshift is constrained worse than 10% for all detectable regions. In Fig. 6, we plot the angle-averaged 90% sky localization uncertainty [35, 40] for IMBH binaries at different redshifts. For binaries at $z \lesssim 0.1$, those with $m_1 \in [10^4, 10^5] M_\odot$ can be localized within $\mathcal{O}(10)$ deg², while binaries with $m_1 \in [10^3, 10^4] M_\odot$ can be localized within around $\mathcal{O}(10^2)$ deg². However, for binaries at $z > 0.5$, all events show poor localization precision.

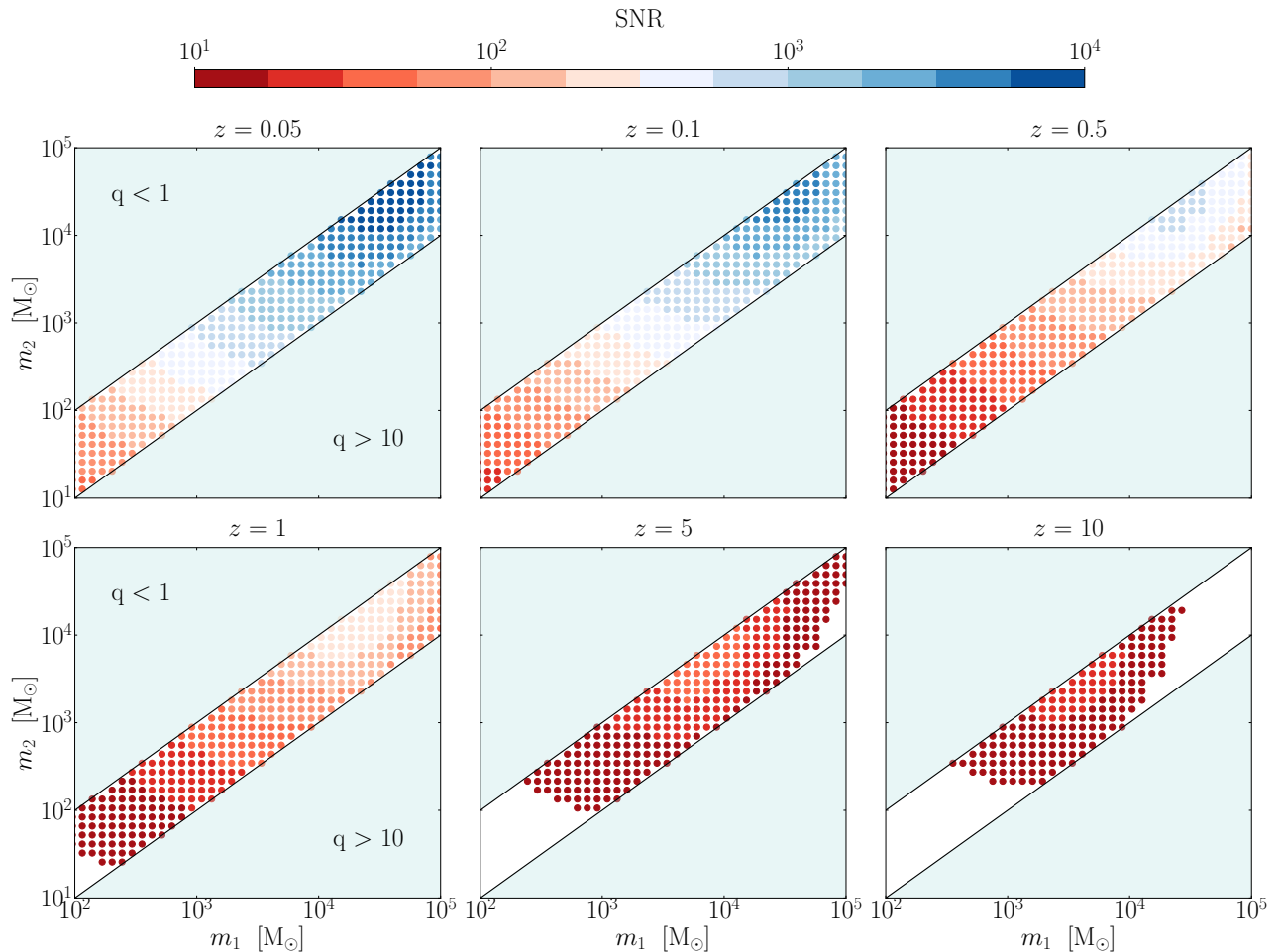


Fig. 2 Each subfigure shows the angle-averaged SNR for binaries fixed at different redshifts. For each point, we take an average of 1000 events which are sampled with priors shown in Table 1. The blank region with no points in the lower subfigures represents the binary systems with angle-averaged SNR < 10.

4 Summary

We explored the detectability of IMBH binaries with the LGWA. Due to its unique shape of the sensitivity curve at decihertz band, the LGWA is more sensitive to distant binaries (i.e. $z \gtrsim 5$) with $m_1 \in [10^3, 10^4] M_\odot$, while preferring nearby binaries (i.e. $z \lesssim 0.5$) with $m_1 \in [10^4, 10^5] M_\odot$. The primary mass can be measured with accuracy better than 0.1% for binaries at $z \lesssim 0.5$, and the redshift can be constrained within 10% for binaries at $z \lesssim 0.1$. Meanwhile, binaries with $m_1 \in [10^4, 10^5] M_\odot$ can be localized within $\mathcal{O}(10) \text{ deg}^2$ at $z \lesssim 0.1$. As the LGWA fills the unexplored GW frequency band between space-borne detectors (i.e., LISA, Taiji, and TianQin) and ground-based detector (i.e., CE and ET), it shows the unique advantage for detecting IMBH binaries. The observations of the inspiral and merger phases of IMBH binaries can offer us more insights into the formation and evolution of black holes, especially bridging the gap between stellar-mass and supermassive black holes [41]. Additionally, it will help us to disentangle the effects between the accretion history and the merger dynamics of black holes [42, 43].

Several recent studies [44–46] showed that the PSD of the LGWA should be updated when carefully considering the lunar response to GWs. We show the updated PSD with the same approach as in Yan et al. [44] in the left panel of Fig. 7, but modify it a little bit using a new sensitivity curve of the LGWA seismometer (we choose the black dotted line as the sensitivity of a single detector, from Fig. 2(b) in Ajith et al. [17]). The updated PSD matches marginally well with the original one in the frequency region lower than 10 mHz but becomes two orders of magnitude worse around decihertz. This variation is primarily because that Yan et al. [44] used the Dyson-type force density, rather than the tidal force density, to calculate the lunar response to GWs. In the right panel of Fig. 7, we show horizon redshift of IMBH binaries for the updated LGWA PSD. Because of the change of sensitivity in the decihertz band, the IMBH binaries now can only be detected up to $z \sim \mathcal{O}(1)$. Finally, more details, including a more precise calculation of the lunar response with the near-surface fine structure of the Moon, need to be considered for future exploration of the science cases with the LGWA.

Acknowledgements. We thank Zhenwei Lyu for helpful discussion and comments. This work was supported by the Beijing Natural Science Foundation (1242018), the National SKA Program of China (2020SKA0120300), the Max Planck Partner Group Program funded by the Max Planck Society, the Fundamental Research Funds for the Central

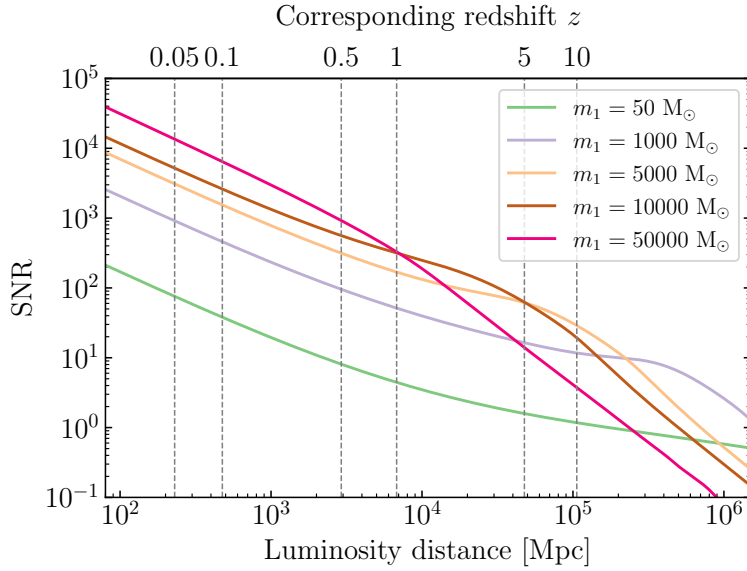


Fig. 3 The evolution of SNR with respect to luminosity distance. These five events have same parameters as in Fig. 1 with corresponding color.

Universities and the High-performance Computing Platform of Peking University. J.Z. is supported by the National Natural Science Foundation of China (No. 12405052) and the Startup Research Fund of Henan Academy of Sciences (No. 241841220). Y.K. is supported by the China Scholarship Council (CSC). X.C. is supported by the Natural Science Foundation of China (No. 12473037).

Author contributions. H.S. contributed to the design, calculation and writing of the initial draft. Y.H. contributed to the sensitivity analysis of the LGWA, and Y.H., Y.K., and J.Z. contributed to discussions and revision of the work. X.C. contributed to the discussion of the results. L.S. initiated the idea, revised the manuscript, and provided supervision and coordination of the whole project.

References

- [1] Abbott, B.P., *et al.*: Observation of Gravitational Waves from a Binary Black Hole Merger. *Phys. Rev. Lett.* **116**(6), 061102 (2016) <https://doi.org/10.1103/PhysRevLett.116.061102> arXiv:1602.03837 [gr-qc]
- [2] Agazie, G., *et al.*: The NANOGrav 15 yr Data Set: Observations and Timing of 68 Millisecond Pulsars. *Astrophys. J. Lett.* **951**(1), 9 (2023) <https://doi.org/10.3847/2041-8213/acda9a> arXiv:2306.16217 [astro-ph.HE]
- [3] Agazie, G., *et al.*: The NANOGrav 15 yr Data Set: Evidence for a Gravitational-wave Background. *Astrophys. J. Lett.* **951**(1), 8 (2023) <https://doi.org/10.3847/2041-8213/acdac6> arXiv:2306.16213 [astro-ph.HE]
- [4] Antoniadis, J., *et al.*: The second data release from the European Pulsar Timing Array I. The dataset and timing analysis. *Astron. Astrophys.* **678**, 48 (2023) <https://doi.org/10.1051/0004-6361/202346841> arXiv:2306.16224 [astro-ph.HE]
- [5] Antoniadis, J., *et al.*: The second data release from the European Pulsar Timing Array II. Customised pulsar noise models for spatially correlated gravitational waves. *Astron. Astrophys.* **678**, 49 (2023) <https://doi.org/10.1051/0004-6361/202346842> arXiv:2306.16225 [astro-ph.HE]
- [6] Antoniadis, J., *et al.*: The second data release from the European Pulsar Timing Array III. Search for gravitational wave signals. *Astron. Astrophys.* **678**, 50 (2023) <https://doi.org/10.1051/0004-6361/202346844> arXiv:2306.16214 [astro-ph.HE]
- [7] Zic, A., *et al.*: The Parkes Pulsar Timing Array third data release. *Publ. Astron. Soc. Austral.* **40**, 049 (2023) <https://doi.org/10.1017/pasa.2023.36> arXiv:2306.16230 [astro-ph.HE]
- [8] Reardon, D.J., *et al.*: Search for an Isotropic Gravitational-wave Background with the Parkes Pulsar Timing Array. *Astrophys. J. Lett.* **951**(1), 6 (2023) <https://doi.org/10.3847/2041-8213/acdd02> arXiv:2306.16215 [astro-ph.HE]
- [9] Xu, H., *et al.*: Searching for the Nano-Hertz Stochastic Gravitational Wave Background with the Chinese Pulsar Timing Array Data Release I. *Res. Astron. Astrophys.* **23**(7), 075024 (2023) <https://doi.org/10.1088/1674-4527/>

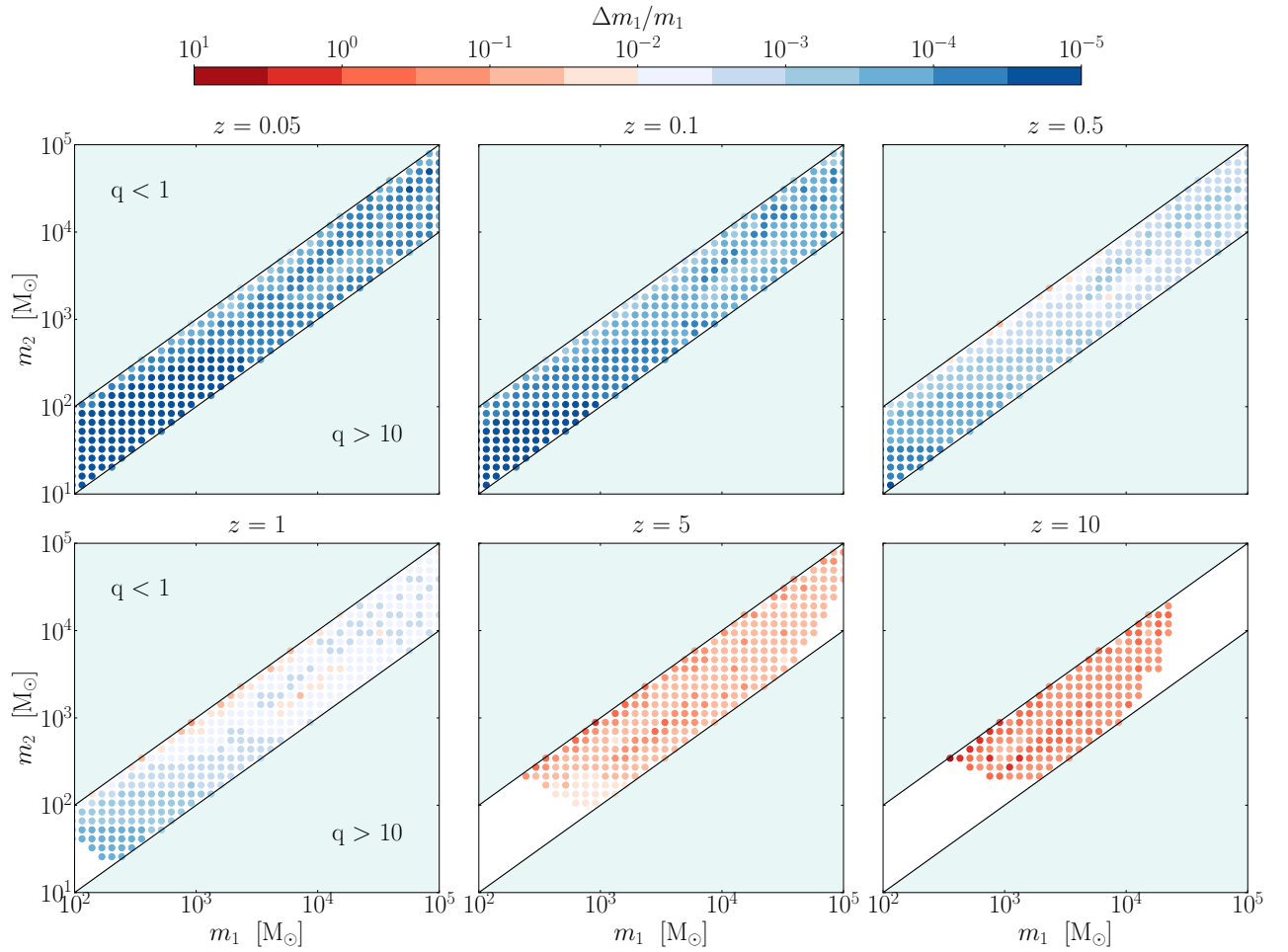


Fig. 4 Same as Fig. 2, but for the angle-averaged relative error of the primary mass, $\Delta m_1/m_1$.

[acdfa5 arXiv:2306.16216](#) [astro-ph.HE]

- [10] Punturo, M., *et al.*: The Einstein Telescope: A third-generation gravitational wave observatory. *Class. Quant. Grav.* **27**, 194002 (2010) <https://doi.org/10.1088/0264-9381/27/19/194002>
- [11] Reitze, D., *et al.*: Cosmic Explorer: The U.S. Contribution to Gravitational-Wave Astronomy beyond LIGO. *Bull. Am. Astron. Soc.* **51**(7), 035 (2019) [arXiv:1907.04833](#) [astro-ph.IM]
- [12] Amaro-Seoane, P., *et al.*: Laser Interferometer Space Antenna. e-prints (2017) [arXiv:1702.00786](#) [astro-ph.IM]
- [13] Hu, W.-R., Wu, Y.-L.: The Taiji Program in Space for gravitational wave physics and the nature of gravity. *Natl. Sci. Rev.* **4**(5), 685–686 (2017) <https://doi.org/10.1093/nsr/nwx116>
- [14] Luo, J., *et al.*: TianQin: a space-borne gravitational wave detector. *Class. Quant. Grav.* **33**(3), 035010 (2016) <https://doi.org/10.1088/0264-9381/33/3/035010> [arXiv:1512.02076](#) [astro-ph.IM]
- [15] Kawamura, S., *et al.*: The Japanese space gravitational wave antenna: DECIGO. *Class. Quant. Grav.* **28**, 094011 (2011) <https://doi.org/10.1088/0264-9381/28/9/094011>
- [16] Harms, J., *et al.*: Lunar Gravitational-wave Antenna. *Astrophys. J.* **910**(1), 1 (2021) <https://doi.org/10.3847/1538-4357/abe5a7> [arXiv:2010.13726](#) [gr-qc]
- [17] Ajith, P., *et al.*: The Lunar Gravitational-wave Antenna: mission studies and science case. *JCAP* **01**, 108 (2025) <https://doi.org/10.1088/1475-7516/2025/01/108> [arXiv:2404.09181](#) [gr-qc]
- [18] Li, J., Liu, F., Pan, Y., Wang, Z., Cao, M., Wang, M., Zhang, F., Zhang, J., Zhu, Z.-H.: Detecting gravitational wave with an interferometric seismometer array on lunar nearside. *Sci. China Phys. Mech. Astron.* **66**(10), 109513 (2023) <https://doi.org/10.1007/s11433-023-2179-9>. [Erratum: *Sci.China Phys.Mech.Astron.* 67, 219551 (2024)]

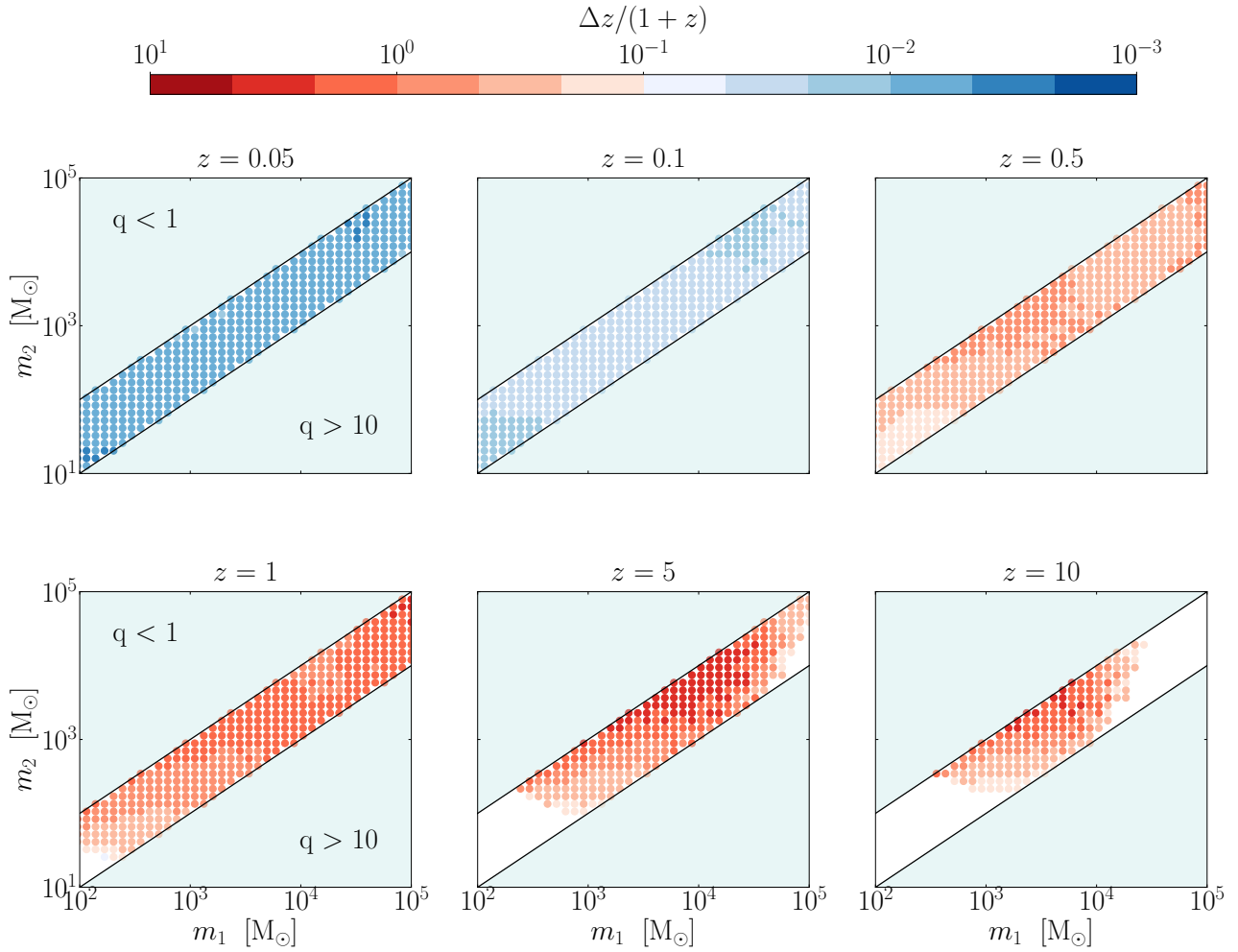


Fig. 5 Same as Fig. 2, but for the angle-averaged relative error of the redshift, $\Delta z/(1+z)$.

- [19] Greene, J.E., Strader, J., Ho, L.C.: Intermediate-Mass Black Holes. *Ann. Rev. Astron. Astrophys.* **58**, 257–312 (2020) <https://doi.org/10.1146/annurev-astro-032620-021835> arXiv:1911.09678 [astro-ph.GA]
- [20] Mezcua, M.: Observational evidence for intermediate-mass black holes. *Int. J. Mod. Phys. D* **26**(11), 1730021 (2017) <https://doi.org/10.1142/S021827181730021X> arXiv:1705.09667 [astro-ph.GA]
- [21] Maggiore, M.: *Gravitational Waves. Vol. 1: Theory and Experiments*. Oxford University Press, Oxford (2007). <https://doi.org/10.1093/acprof:oso/9780198570745.001.0001>
- [22] Will, C.M.: On the rate of detectability of intermediate-mass black-hole binaries using LISA. *Astrophys. J.* **611**, 1080 (2004) <https://doi.org/10.1086/422387> arXiv:astro-ph/0403644
- [23] Arca-Sedda, M., Amaro-Seoane, P., Chen, X.: Merging stellar and intermediate-mass black holes in dense clusters: implications for LIGO, LISA, and the next generation of gravitational wave detectors. *Astron. Astrophys.* **652**, 54 (2021) <https://doi.org/10.1051/0004-6361/202037785> arXiv:2007.13746 [astro-ph.GA]
- [24] Stokov, V., Fragione, G., Berti, E.: LISA constraints on an intermediate-mass black hole in the Galactic Centre. *Mon. Not. Roy. Astron. Soc.* **524**(2), 2033–2041 (2023) <https://doi.org/10.1093/mnras/stad2002> arXiv:2303.00015 [astro-ph.HE]
- [25] Liu, S., Wang, L., Hu, Y.-M., Tanikawa, A., Trani, A.A.: Merging hierarchical triple black hole systems with intermediate-mass black holes in population III star clusters. *Mon. Not. Roy. Astron. Soc.* **533**(2), 2262–2281 (2024) <https://doi.org/10.1093/mnras/stae1946> arXiv:2311.05393 [astro-ph.GA]
- [26] Sedda, M.A., *et al.*: The missing link in gravitational-wave astronomy: discoveries waiting in the decihertz range. *Class. Quant. Grav.* **37**(21), 215011 (2020) <https://doi.org/10.1088/1361-6382/abb5c1> arXiv:1908.11375 [gr-qc]

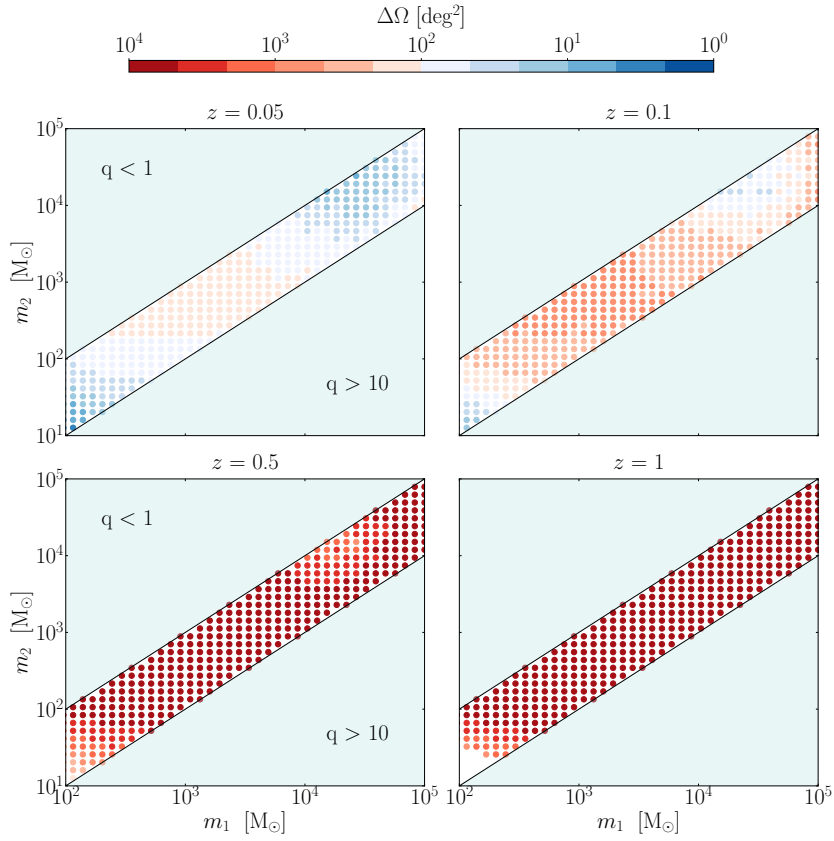


Fig. 6 Same as Fig. 2, but for the angle-averaged 90% sky localization errors at different redshifts, $z \in \{0.05, 0.1, 0.5, 1\}$.

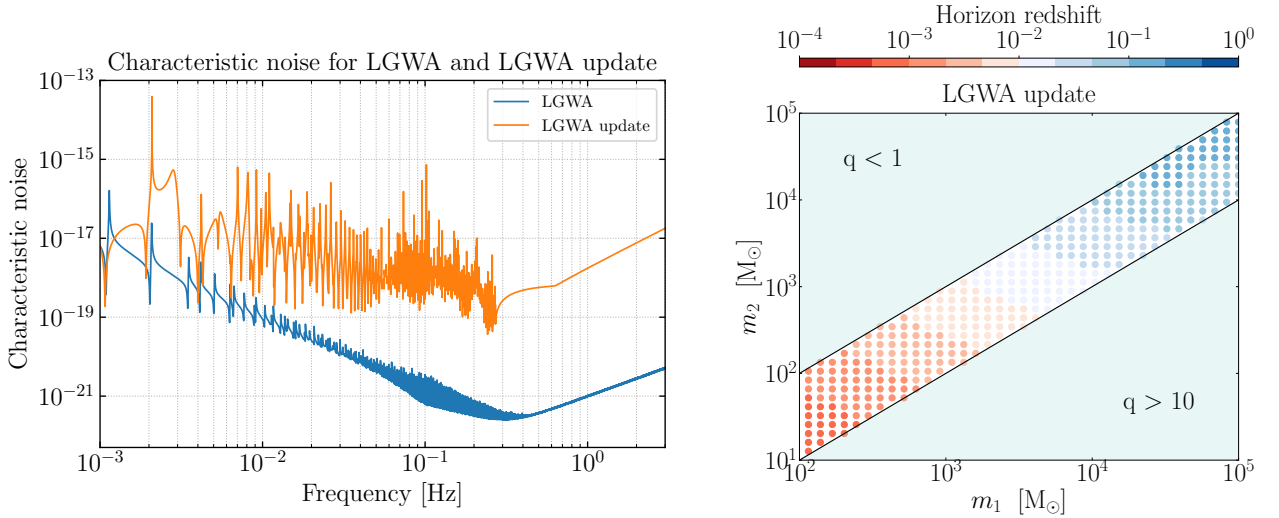


Fig. 7 The left panel shows the characteristic noise h_n for LGWA and LGWA update. The right panel shows the horizon redshift same to Fig. 1 but here for LGWA update.

- [27] Graff, P.B., Buonanno, A., Sathyaprakash, B.S.: Missing Link: Bayesian detection and measurement of intermediate-mass black-hole binaries. *Phys. Rev. D* **92**(2), 022002 (2015) <https://doi.org/10.1103/PhysRevD.92.022002> [arXiv:1504.04766](https://arxiv.org/abs/1504.04766) [gr-qc]
- [28] Veitch, J., Pürrer, M., Mandel, I.: Measuring intermediate mass black hole binaries with advanced gravitational wave detectors. *Phys. Rev. Lett.* **115**(14), 141101 (2015) <https://doi.org/10.1103/PhysRevLett.115.141101> [arXiv:1503.05953](https://arxiv.org/abs/1503.05953) [astro-ph.HE]
- [29] Han, W.-B., Cao, Z., Hu, Y.-M.: Excitation of high frequency voices from intermediate-mass-ratio inspirals with large eccentricity. *Class. Quant. Grav.* **34**(22), 225010 (2017) <https://doi.org/10.1088/1361-6382/aa891b> [arXiv:1710.00147](https://arxiv.org/abs/1710.00147) [gr-qc]

- [30] Huerta, E.A., Gair, J.R.: Intermediate-mass-ratio-inspirals in the Einstein Telescope. II. Parameter estimation errors. *Phys. Rev. D* **83**, 044021 (2011) <https://doi.org/10.1103/PhysRevD.83.044021> [arXiv:1011.0421](https://arxiv.org/abs/1011.0421) [gr-qc]
- [31] Reali, L., Cotesta, R., Antonelli, A., Kritos, K., Stokov, V., Berti, E.: Intermediate-mass black hole binary parameter estimation with next-generation ground-based detector networks. *Phys. Rev. D* **110**(10), 103002 (2024) <https://doi.org/10.1103/PhysRevD.110.103002> [arXiv:2406.01687](https://arxiv.org/abs/2406.01687) [gr-qc]
- [32] García-Quirós, C., Colleoni, M., Husa, S., Estellés, H., Pratten, G., Ramos-Buades, A., Mateu-Lucena, M., Jaume, R.: Multimode frequency-domain model for the gravitational wave signal from nonprecessing black-hole binaries. *Phys. Rev. D* **102**(6), 064002 (2020) <https://doi.org/10.1103/PhysRevD.102.064002> [arXiv:2001.10914](https://arxiv.org/abs/2001.10914) [gr-qc]
- [33] Whelan, J.T.: The geometry of gravitational wave detection. *LIGO Document Control Center* (2013)
- [34] Branchesi, M., *et al.*: Lunar Gravitational-Wave Detection. *Space Sci. Rev.* **219**(8), 67 (2023) <https://doi.org/10.1007/s11214-023-01015-4>
- [35] Dupletsa, U., Harms, J., Banerjee, B., Branchesi, M., Goncharov, B., Maselli, A., Oliveira, A.C.S., Ronchini, S., Tissino, J.: gwfish: A simulation software to evaluate parameter-estimation capabilities of gravitational-wave detector networks. *Astron. Comput.* **42**, 100671 (2023) <https://doi.org/10.1016/j.ascom.2022.100671> [arXiv:2205.02499](https://arxiv.org/abs/2205.02499) [gr-qc]
- [36] Yan, H., Chen, X., Zhang, J., Zhang, F., Shao, L., Wang, M.: Constraining the stochastic gravitational wave background using the future lunar seismometers. *Phys. Rev. D* **110**(4), 043009 (2024) <https://doi.org/10.1103/PhysRevD.110.043009> [arXiv:2405.12640](https://arxiv.org/abs/2405.12640) [gr-qc]
- [37] Finn, L.S.: Detection, measurement and gravitational radiation. *Phys. Rev. D* **46**, 5236–5249 (1992) <https://doi.org/10.1103/PhysRevD.46.5236> [arXiv:gr-qc/9209010](https://arxiv.org/abs/gr-qc/9209010)
- [38] Borhanian, S.: GWBENCH: a novel Fisher information package for gravitational-wave benchmarking. *Class. Quant. Grav.* **38**(17), 175014 (2021) <https://doi.org/10.1088/1361-6382/ac1618> [arXiv:2010.15202](https://arxiv.org/abs/2010.15202) [gr-qc]
- [39] Moore, C.J., Cole, R.H., Berry, C.P.L.: Gravitational-wave sensitivity curves. *Class. Quant. Grav.* **32**(1), 015014 (2015) <https://doi.org/10.1088/0264-9381/32/1/015014> [arXiv:1408.0740](https://arxiv.org/abs/1408.0740) [gr-qc]
- [40] Li, Y., Heng, I.S., Chan, M.L., Messenger, C., Fan, X.: Exploring the sky localization and early warning capabilities of third generation gravitational wave detectors in three-detector network configurations. *Phys. Rev. D* **105**(4), 043010 (2022) <https://doi.org/10.1103/PhysRevD.105.043010> [arXiv:2109.07389](https://arxiv.org/abs/2109.07389) [astro-ph.IM]
- [41] Sesana, A., Gair, J., Berti, E., Volonteri, M.: Reconstructing the massive black hole cosmic history through gravitational waves. *Phys. Rev. D* **83**, 044036 (2011) <https://doi.org/10.1103/PhysRevD.83.044036> [arXiv:1011.5893](https://arxiv.org/abs/1011.5893) [astro-ph.CO]
- [42] Sesana, A., Haardt, F., Madau, P.: Interaction of massive black hole binaries with their stellar environment. 3. Scattering of bound stars. *Astrophys. J.* **686**, 432 (2008) <https://doi.org/10.1086/590651> [arXiv:0710.4301](https://arxiv.org/abs/0710.4301) [astro-ph]
- [43] Klein, A., *et al.*: Science with the space-based interferometer eLISA: Supermassive black hole binaries. *Phys. Rev. D* **93**(2), 024003 (2016) <https://doi.org/10.1103/PhysRevD.93.024003> [arXiv:1511.05581](https://arxiv.org/abs/1511.05581) [gr-qc]
- [44] Yan, H., Chen, X., Zhang, J., Zhang, F., Wang, M., Shao, L.: Toward a consistent calculation of the lunar response to gravitational waves. *Phys. Rev. D* **109**(6), 064092 (2024) <https://doi.org/10.1103/PhysRevD.109.064092> [arXiv:2403.08681](https://arxiv.org/abs/2403.08681) [gr-qc]. [Erratum: *Phys.Rev.D* 109, 089903 (2024)]
- [45] Belgacem, E., Maggiore, M., Moreau, T.: Coupling elastic media to gravitational waves: an effective field theory approach. *Journal of Cosmology and Astroparticle Physics* **2024**(7), 028 (2024) <https://doi.org/10.1088/1475-7516/2024/07/028> [arXiv:2403.16550](https://arxiv.org/abs/2403.16550) [gr-qc]
- [46] Majstorović, J., Vidal, L., Lognonné, P.: Modeling lunar response to gravitational waves using normal-mode approach and tidal forcing. *arXiv e-prints*, 2411–09559 (2024) <https://doi.org/10.48550/arXiv.2411.09559> [arXiv:2411.09559](https://arxiv.org/abs/2411.09559) [gr-qc]